Journal of Molecular Structure 1231 (2021) 129923

Contents lists available at ScienceDirect

Journal of Molecular Structure

journal homepage: www.elsevier.com/locate/molstr

Synthesis, characterization and DFT investigation of new metal complexes of Ni(II), Mn(II) and VO(IV) containing N,O-donor Schiff base ligand

Djouhra Aggoun[a,b,*], Zakia Messasma[a], Brahim Bouzerafa[c], Raúl Berenguer[d], Emilia Morallon[d], Yasmina Ouennoughi[a], Ali Ourari[a]

[a] Laboratoire d'Électrochimie, d'Ingénierie Moléculaire et de Catalyse Redox (LEIMCR), Faculté de Technologie, Université Ferhat ABBAS de Sétif-1, Sétif 19000, Algeria
[b] Département de chimie, Faculté des sciences, Université Ferhat ABBAS de Sétif-1, Sétif 19000, Algeria
[c] Laboratoire de Préparation, Modification des Matériaux Polymériques Multiphasiques (LMPMP), Faculté de Technologie, Université Ferhat ABBAS Sétif-1, 19000 Sétif, Algeria
[d] Departamento de Química Física, Instituto Universitario de Materiales, Universidad de Alicante (UA), Ap.99, 03080 Alicante, Spain

ARTICLE INFO

Article history:
Received 30 October 2020
Revised 5 January 2021
Accepted 6 January 2021
Available online 11 January 2021

Keywords:
N,O donors ligand
Bis-bidentate Schiff base complexes
Spectral studies
Cyclic voltammetry
Thermogravimetry
DFT calculations

ABSTRACT

In this work, a bidentate Schiff base ligand (**HL**) containing N and O as donor heteroatoms has been used to synthesize series of new stable metal complexes of general composition of $\mathbf{M(L)_2}$ with M = Mn, Ni and VO. This ligand was obtained from condensation of 2-methoxybenzylamine on 2,3-dihydroxybenzaldehyde in methanolic solutions in which its complexes were obtained by mixing the corresponding metal acetate salt and the ligand in 1:2 molar ratio. The resulting three complexes have been characterized by different analytical techniques like FT-IR, UV-Vis, mass spectroscopy, thermogravimetry and cyclic voltammetry, to identify their molecular structures and redox/electrochemical properties. Moreover, the effect of the metal on the complexes electronic properties with their reactivity has also been studied by Density Functional Theory (DFT). The stable structures were optimized by using the hybrid B3LYP/6–31 G method. The spectroscopic data obtained suggest that the metal is bonded to the ligand through the phenolic-like oxygen and the imine-type nitrogen atoms. Electronic and vibrational absorption spectra of the nickel complex was found to be of square-planar geometry while square-pyramidal and octahedral geometries have been proposed for VO(IV) and Mn(II) complexes, respectively. The thermogravimetric analyses of these complexes confirmed the presence of water molecules in their structures and thermal decomposition led to the formation of metal oxides as the latest residues. The voltammogram of the Ni(II) complex suggests the existence of quasi-reversible redox system in DMSO solution.

1. Introduction

In recent decades, Schiff bases ligands [1] have attracted a significant attention from academic researchers not only for their structural variety (fundamental research), but also for their various physicochemical properties opening a wide domain of applications (practical point of view) [2]. This interest is as well due to the structural versatility of Schiff bases for their efficient use as asymmetric compounds (Katsuki and Jacobsen) and stabilizer agents for different complexes in their diverse oxidation states and controlling the performance of metals in a large variety of useful transformations [3,4]. Moreover, the coordination geometry of these complexes [5,6] depends upon various factors, including the size of coordination sphere, electronic configuration of the central metal ions, non-bonding interactions between atoms in different ligands, accompanied with inherent rigidity due to the presence of aromatic rings.

Since they are getting increasing significance as analytical and electroanalytical reagents [7,8], the transition metal complexes employing chelating agents like Schiff bases were found to be as elegant alternative for the porphyrinic ligands in coordination chemistry. Their importance was also clearly proved by their efficient catalytical activities in numerous photochemical, chemical or electrochemical reactions [9-13] especially, the transition metal complexes containing N,O-heteroatoms utilized as source of electrons

* Corresponding author.
E-mail address: djouhra.aggoun@univ-setif.dz (D. Aggoun).

https://doi.org/10.1016/j.molstruc.2021.129923
0022-2860/

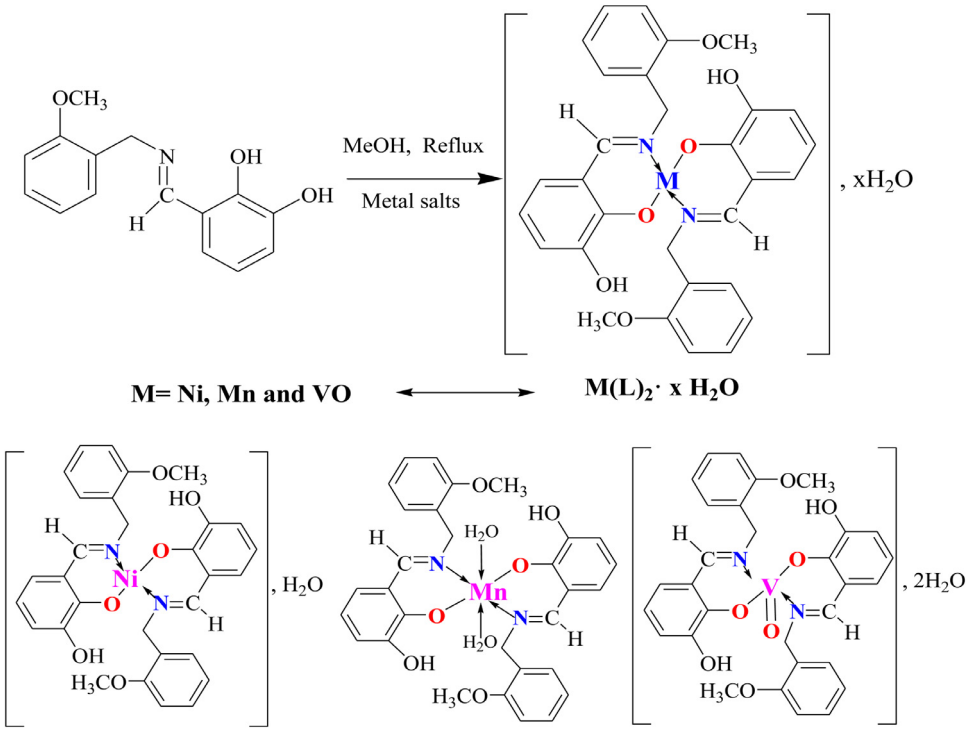

Scheme 1. Scheme of the synthesis of new complexes of Ni(II), Mn(II) and VO(IV) with the bidentate Schiff-base ligand.

involved in the coordination process [14-16]. This is essential in organic chemistry as starting materials, synthetic intermediates and designer molecules for the materials science field and industry of chemicals and bioactive substances. In addition, they have played a seminal role in the development of modern coordination chemistry, but they could also play a crucial role in the development of inorganic chemistry.

The design of new bidentate Schiff base ligands implicating N and O atoms as functional groups with their electrons donor capability is again very interesting for metal complexation route since, these ligands can be prepared by condensation of aldehydes on primary amines. Among different preparation methods, we have previously reported the synthesis of novel N,O-donor Schiff base ligands from the combination of benzaldehydes with phenylamines [5,14-16]. The donor capability of these ligands can be further tailored by modifying the nature and relative positions of different substituents in these precursor compounds. Hence, new metal complexes exhibiting different properties can be derived from these new ligands [17,18]. In a previous work, we have demonstrated that a Schiff base ligand, obtained from 2-methoxybenzylamine and 2,3-dihydroxybenzaldehyde, can actually be coordinated and detected as complex species of Cu^{2+}, Co^{2+}, Fe^{2+} and Fe^{3+} ions by color changes [5]. Despite not studied yet, this type of Schiff base ligands could also form interesting complexes with other redox active species.

Continuing our efforts in the synthesis and study of new transitions metal complexes, this work reports the synthesis and physicochemical and electrochemical characterization of three new complexes of Ni(II), Mn(II) and VO(IV) (oxovanadium), derived from 2-methoxybenzylamine and 2,3-dihydroxybenzaldehyde. Specifically, this study is essentially focused on the elucidation of their molecular structures accompanying the crystallization geometries with exploring their induced redox properties.

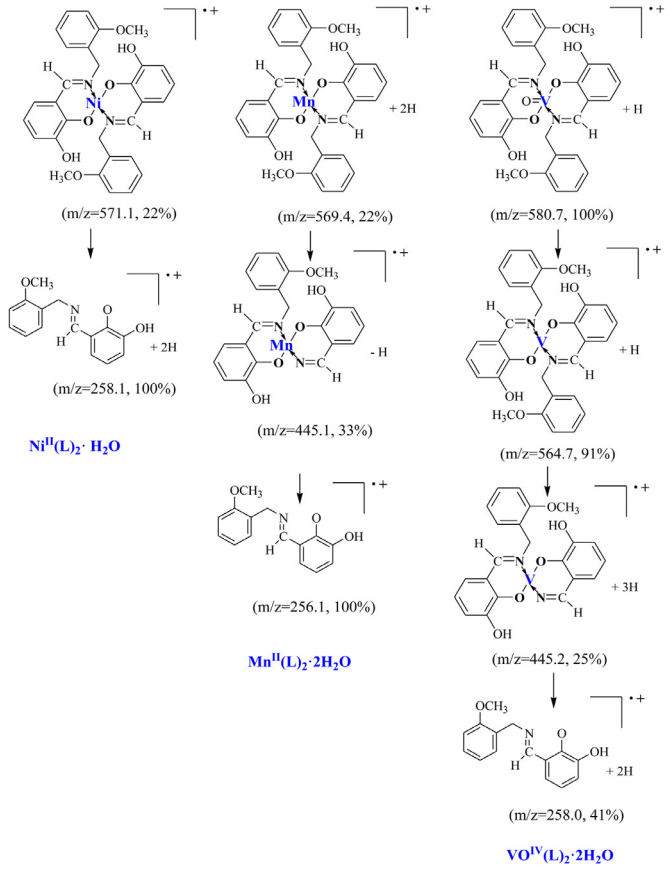

Scheme 2. Proposed major fragments ions deduced from the mass spectra of Ni(II), Mn(II) and VO(IV) complexes.

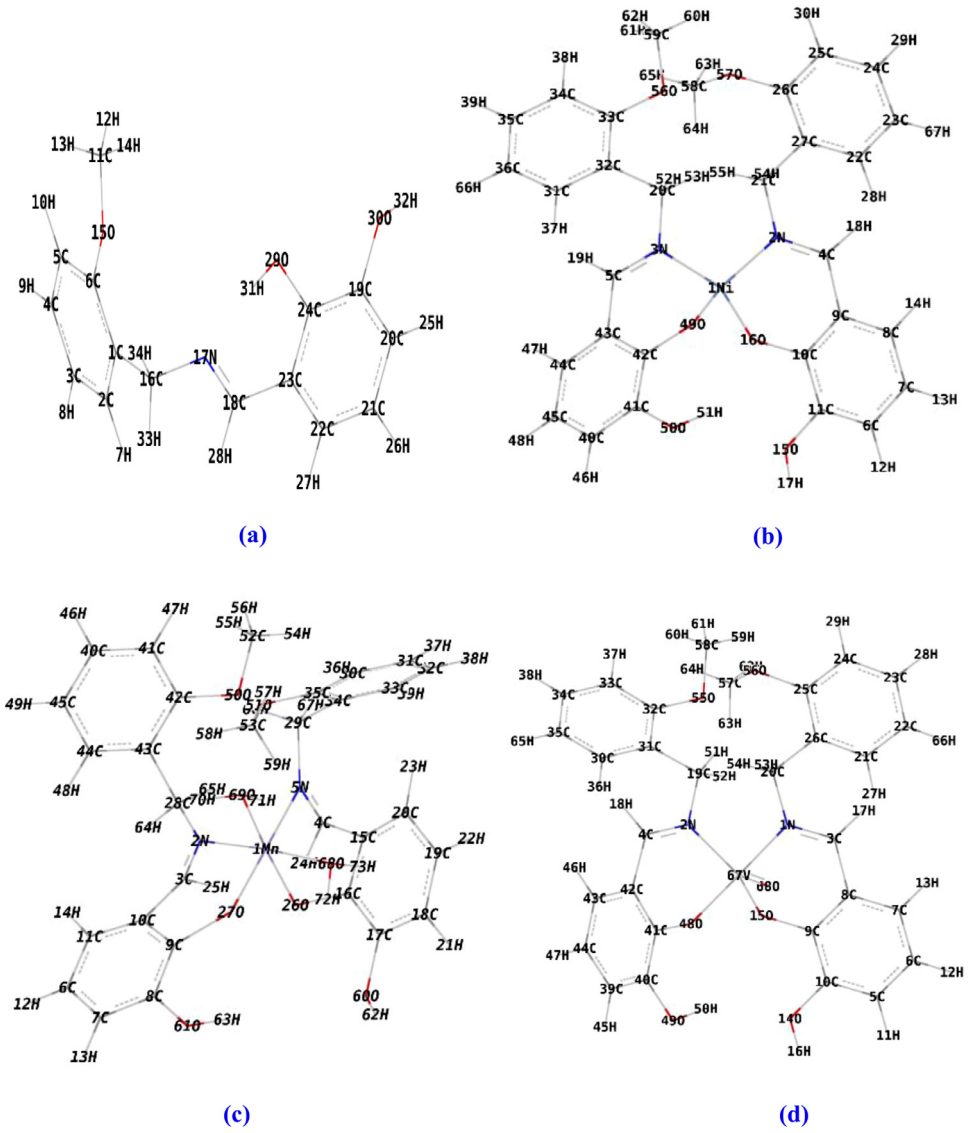

Scheme 3. Numbering Scheme of the optimized structures of **(a)** Ligand HL, **(b)** Complex Ni(II), **(c)** Complex Mn(II), **(d)** Complex VO(IV).

2. Experimental

2.1. Materials

All the chemicals were purchased from commercial sources and used without any further purification. The purity of the synthesized compounds was checked by thin-layer chromatography (TLC) using glass plates precoated with silica gel (60F; Merck).

2.2. Synthesis of the Schiff base ligand and its complexes

The Schiff-base ligand (HL) was prepared according the literature [5]. Briefly, 1 mmol of 2-methoxyphenylmethylamine was mixed with 1 mmol of the 2,3-dihydroxybenzaldehyde in methanol (10 mL). The resulting solution was refluxed for ca. 2 h and allowed to cooling. The yellow powder ligand was used to obtain the new metal complexes. For these complexes, the required weights of the acetate salts of Ni(II) ($Ni(CH_3COO)_2 \bullet 4H_2O$), Mn(II) ($Mn(CH_3COO)_2 \bullet 4H_2O$) and VO(IV) ($VO(CH_3COO)_2$), dissolved in absolute MeOH, were added to a refluxed solution of the ligand (HL) dissolved in the same solvent wih 1:2 molar ratio of metal:ligand, respectively. The resulting mixture was stirred under reflux for 4 h until the complete formation of the complexes as precipitates. These precipitates were then collected by filtration, washed several times with cold ethanol and then with diethylether to remove any traces of unreacted starting materials, and finally dried in a vacuum desiccator, which leads to the targeted metal complexes. The synthesis of the different complexes and their molecular structures, as proposed from the data obtained in this work (see Section 3), are shown in the following Scheme 1.

2.3. Physico-chemical and electrochemical characterization

The obtained complexes were characterized by elemental analysis by using a (C, N, H, S) LECO analyzer (Micro TruSpec model). This analysis was repeated three times to confirm the reproducibility of the results.

FT-IR spectra of the complexes were recorded by preparing KBr pellets on a Perkin-Elmer 1000 FTIR Spectrophotometer. UV-Visible spectroscopy was carried out in DMF solutions on a UNICAM UV-300 spectrophotometer (path length of the cell, 1 cm). For mass spectrometry (LC-MS), a HPLC Agilent 1100 series coupled to UV-Vis and MS with ionic tramp detector (Agilent model 1100 Series LC/MSD Trap SL) was used.

Thermal analysis (TG and DTG) of the complexes was obtained under nitrogen atmosphere using a TGA Perkin Elmer thermal analyzer. The heating rate was set at 10 °C min^{-1} and the weight loss was measured from 25 °C up to 950 °C. Cyclic voltammetry was utilized to study the redox and electrochemical properties of the complexes. The experiments were carried out in an undivided Metrohm cell of 5 cm^3 using a Voltalab 40 (potentiostat/galvanostat) PGZ 301 A 0.1 M of tetra-n-butylammonium tetrafluoroborate ($TBABF_4$) solutions in dimethyl sulfoxide (DMSO) was used as supporting electrolyte in all the electrochemical experiments. The planar tip of a glassy carbon (GC) bar (Ø, 3 mm) was used as working electrode, a platinum wire (Pt) as auxiliary electrode and all the electrode potentials were referred versus a saturated calomel electrode (SCE), taken as reference electrode. Furthermore, the influence of different scan rates: 25, 50, 75, 100, 200, 300, 400 and 500 mV/s, has been here applied.

2.4. Computational study

Theoretical calculations for HL ligand and its Ni(II), Mn(II) and VO(IV) complexes were performed using the Gaussian 09 program, based on Density Functional Theory (DFT) [19], using Beck's three parameter hybrid exchange functional [20], with Lee-Yang-Parr correlation functional (B3LYP) and 6–31 G (d, p) basis set [21,22]. In order to make comparative study between the ligand and their complexes with the optimized configurations, HOMO, LUMO, gap properties and Energy calculations for the compounds were useful to determine binding sites and predicting the reactivity of the compounds. The Molecular electrostatic potential (MEP) and the global reactivity descriptors of the molecules were also performed by the DFT.

3. Results and discussion

3.1. Physico-chemical properties and molecular formula of the complexes

The obtained complexes were intensively colored, stable in air and moisture free powder solids. The Ni(II), Mn(II), and VO(IV) complexes were not soluble in most common solvents, such as water like methanol, ethanol, ethyl acetate and acetonitrile. However, they were fairly soluble in N,N-dimethyl formamide (DMF) and dimethyl sulfoxide (DMSO). Table 1 summarizes some of the physico-chemical properties and molecular formulae of the complexes. As it can be deduced from this table, the results of elemental analysis (measured) were found to be in good agreement with those calculated from the proposed molecular formulae for the different synthesized complexes.

3.2. Spectroscopic characterizations of the complexes

3.2.1. FT-IR spectroscopy

Fig. 1 shows the FT-IR spectra of the synthesized complexes, whereas Table 2 collects the wavelength of some of the bands assigned to the stretching and bending vibrations. The FT-IR spectra of all complexes (Fig. 1) display bands between 3650 and 3200 cm^{-1} due to ν(OH) of crystalline or coordinated water molecules associated with each complex. The absorption bands observed in the region 3100–2900 cm^{-1} may be due to the aromatic and aliphatic ν(C–H), respectively [24], whereas the bands seen between 1050 and 1020 cm^{-1} may correspond to ν(C–O–C) stretching vibration of the methoxy group [23]. In addition, the complexes possessed a potential donor site, like the azomethine group (–C=N), which has tendency to coordinate metal ions. The strong bands associated to this group are generally situated between 1660 and 1630 cm^{-1} [25]. Specifically, for the studied ligand, this band

Table 1
Physico-chemical properties and proposed molecular formulae of the synthesized Ni(II), Mn(II) and VO(IV) Schiff base complexes.

Complexes	$\lambda_{max(n)}$ (nm)[a]		$\varepsilon_{max(n)}$ ($M^{-1}.cm^{-1}$)[b]	LC-MS (m/z)[c]		Elemental analysis[d] C (%)	H(%)	N(%)	Molecular formula
$Ni^{II}(L)_2{\cdot}H_2O$	(1)	276	(1) 16,250	571.1	$[NiL_2]^+$	60.84 (61.15)	4.88 (5.13)	4.68 (4.75)	$C_{30}H_{30}N_2O_7Ni$
	(2)	380	(2) 3820						
$Mn^{II}(L)_2{\cdot}2H_2O$	(1)	329	(1) 10,600	569.4	$[MnL_2 + 2H^+]$	60.27 (59.7)	4.43 (5.34)	4.23 (4.64)	$C_{30}H_{32}N_2O_8Mn$
	(2)	585	(2) 890						
$VO^{IV}(L)_2{\cdot}2H_2O$	(1)	269	(1) 18,600	580.7	$[VOL_2 + H^+]$	58.08 (58.54)	4.62 (5.24)	3.47 (4.55)	$C_{30}H_{32}N_2O_9V$
	(2)	310	(2) 15,830						
	(3)	430	(3) 4560						

[a] Wavelength of maximum absorbance;.
[b] Molar attenuation coefficient;.
[c] Some of the major fragmentation peaks observed on the mass spectra of nickel(II), manganese(II) and oxovanadium(IV) complexes;.
[d] Measured C, H, N contents (atomic%) in the complexes and the calculated ones (in brackets) from the proposed molecular formulae.

Table 2
Characteristic FT-IR bands (4000–400 cm^{-1}) of the synthesized complexes.

Complex	ν(O–H)	ν(C–H) (arom.)	ν(C–H) (aliph.)	ν(C=N)	ν(C–O)	ν(C–O-C)	ν(V=O)	ν(M-O)	ν(M-N)
Nickel	3600–3200	3077	2951	1638	1247	1043	-	552	445
Manganese	3620–3200	3079	2945	1658	1253	1030	-	538	450
Oxovanadium	3650–3200	3080	2950	1658	1253	1023	970	531	443

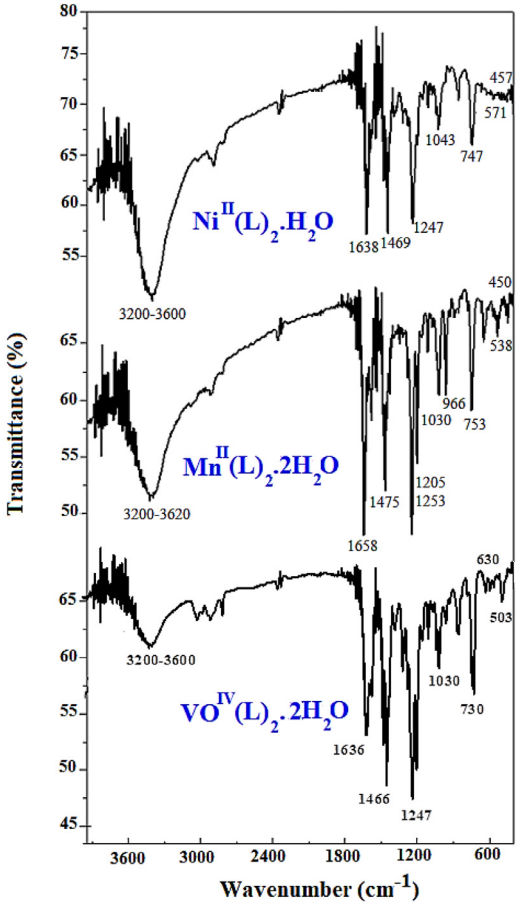

Fig. 1. FT-IR Spectra of the obtained Ni(II), Mn(II) and VO(IV) Schiff base complexes.

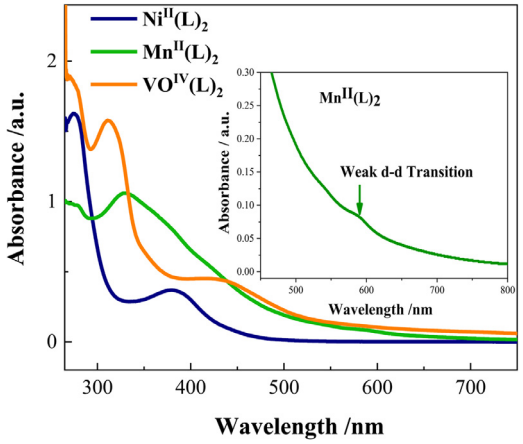

Fig. 2. UV-Vis Spectra of the obtained Ni(II), Mn(II) and VO(IV) Schiff base complexes.

was observed at 1644 cm^{-1} [5], but it is found to be shifted to the lower frequencies by about 6 cm^{-1} in the spectrum of the nickel complex, and then shifted to the higher frequencies by almost 14 cm^{-1} in the spectra of the manganese and oxovanadium complexes. This result suggests that the azomethine nitrogen may be coordinated to the metallic centers. Additionally, the absorption bands seen 1247–1253 cm^{-1} range are assigned to C–O stretch of the phenolate groups in the complexes. These bands show a neat displacement to the higher frequencies compared with the value of this band in the corresponding ligand appearing at about 1240 cm^{-1} [5] in compliance with deprotonation followed by its bonding of the oxygen atom of phenolate to the metallic ions [26].

In the oxovanadium complex, a strong band at 970 cm^{-1} was observed, it can be assigned to ν(V=O) vibrations [27]. The coordination of the Schiff base ligands to the metal ions is also confirmed by the appearance of new bands in the spectra of metal complexes in the range of 460–440 cm^{-1}, attesting the coordination of metal ions to the azomethinic groups ν(M-N) [28]. Another absorption band was also seen, not far from the previous ν(M-N) frequency, in the region of 560–530 cm^{-1} corresponding to ν(M-O) bond [28]. Taking into account of these results, it can be inferred that the two Schiff base molecules coordinating the metallic centers in the three complexes may act as dibasic bis-bidentate ligands.

3.2.2. UV-Vis Spectroscopy

Electronic (UV–Vis) spectra of all complexes have been recorded in DMF solutions [10^{-4} M] (Fig. 2). For all the complexes, an absorption band relatively intense was observed between 260 and 280 nm. This absorption band could be ascribed to the π–π^* transitions of aromatic rings and azomethine groups. In the case of the electronic spectrum of nickel complex, another new band was as well seen at 380 nm. This band is assigned to the ligand-metal charge-transfer (LMCT) transition $O_{phenolate} \rightarrow$ Ni(II).

As for the spectrum of manganese complex, two bands are observed. The first, located at 329 nm, is characteristic of the charge-transfer (LMCT) transition Mn(III)→$O_{phenolate}$ and it appears as shifted to the higher energy when compared to its equivalent band of nickel complex [29,30]. The second one appears as a broad band centered at 585 nm. This electronic transition is attributed to a charge-transfer (LMCT) between pπ-orbital of the ligand and dπ-orbital of Mn(II) [31,32]. Regarding the spectrum of oxovanadium complex, it shows two types of transitions. The first absorption band was observed at 310 nm corresponding to n–π^* transitions, while the second one at 430 nm is attributable to the charge-transfer (LMCT) transition from the oxygen atom of phenolate group ($O_{phenolate}$) to the empty *d* orbital's on the vanadium ion [33,34]. Accordingly, upon coordination, these observed absorption bands appear between 320 and 600 nm corresponding to the square planar geometry for Ni(II) complex [35], octahedral geometry for Mn(II) complex [36] and finally square-pyramidal geometry for VO(IV) complex [37].

3.2.3. Mass spectrometry

Mass spectrometry is potentially considered as a powerful structural characterization technique in molecular chemistry. This technique has also been successfully applied in coordination chemistry to elucidate the major molecular ion peaks of our synthesized Schiff base complexes. This analysis was carried out by HPLC chromatography coupled with mass spectrometry technique (LC-MS).

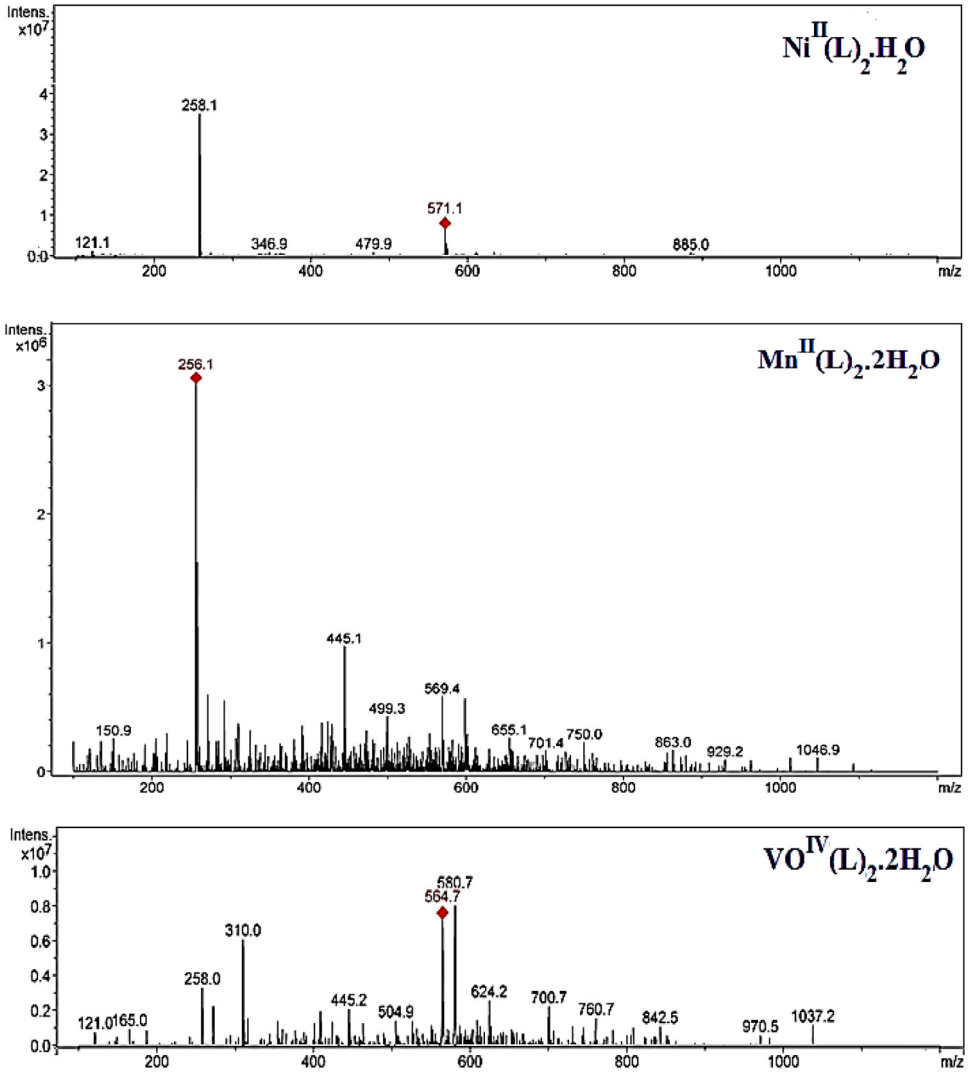

Fig. 3. Mass spectra of Ni(II), Mn(II) and VO(IV) Schiff base complexes.

The mass spectrum of nickel complex (Fig. 3) displays a fragmentation ion peak expressed with m/z = 571.1, which may correspond to the parent molecular ion peak $[Ni^{(II)}L_2]^+$ (calc. 571.2). On the other hand, a base peak with m/z equal to 258.1 was observed. This could be assigned to the mass of ligand diprotonated $[L + 2H]^+$. The molecular structure deduced from these mass fragmentation patterns is included in the Scheme 2.

As for the mass spectrum of the manganese complex, it shows a molecular ion peak with m/z ratio equal to 569.4. This fragment ion may fit with the molecular weight of the expected compound. Moreover, another important fragment with m/z ratio = 445.1 (33.4%) is also observed, which may correspond to the $[C_{21}H_{19}O_5Mn - H]^+$ ion (Scheme 2). The fragment with m/z = 256.1, with a relative abundance of 100%, is assigned to the ligand $[L]^+$, confirming its high stability and therefore, clearly corresponds to its base peak.

For the last complex of oxovanadium, it exhibits a strong peak at m/z = 580.7 (100%), which may be indicative of the molecular peak and also the base peak, confirming its high thermodynamic stability by a simple fixation of the oxygen atom on the metallic center. This behavior seems to be the main particularity for this complex when compared to its both analogs such as Ni(II) and Mn(II). In addition, the mass spectrum of this compound shows again multiple peaks representing successive degradation of this complex leading to the formation of different fragments (Scheme 2), highlighting among them the Schiff base ligand ion peak $[L]^+$ for which m/z ratio is equal to 258.0 (41.0%).

So, all these results confirmed that the synthesized complexes are mononuclear, with two molecular moieties of Schiff base ligands, and they are, therefore, in good agreement with their proposed molecular structures shown in the Scheme 1.

3.3. Thermogravimetric analysis (TG/DTG)

Fig. 4 shows the TG and DTG curves recorded for the three metal complexes. As it is observed, upon increasing the temperature, the complexes showed a gradual weight loss. Generally, this weight loss can be initially assigned to the release of water molecules, followed by other successive decompositions leading to the formation of metallic oxides as latest forms of degradation. Different decomposition stages, temperature ranges, DTG peak positions, as well as the experimental and calculated mass loss percentages for these complexes are summarized in Table 3.

First, the thermogram of nickel complex undergoes decomposition in four steps (Fig. 4A). The first one is accompanied by a weight loss of 3.80%, corresponding to the release of one molecule of water theoretically calculated as 3.05%. The DTG curve of the second step, for which the temperatures ranged from 220.0 to

Table 3
Thermal decomposition data for the prepared complexes.

Samples	Number of steps	Temp. range / °C	T_{max}/ °C	Mass loss /% Found (Calcd.)	Assignments	Residue/% Found (Calcd.)
$Ni^{II}(L)_2 \bullet H_2O$	4	125.9–173.4	144.6	3.8(3.05)	Loss of H_2O	
		220.6–300.0	242.0	17.7(18.15)	Loss of C_7H_7O	
		337.9–450.3	396.8	13.0(12.89)	Loss of C_6H_4	41.3 (41.41)
		522.6–613.6	557.4	24.2(24.6)	Loss of $C_3H_{17}N_2O_4$	NiO+ 16C
$Mn^{II}(L)_2 \bullet 2H_2O$	4	138.6–222.5	181.6	3.0(2.98)	Loss of H_2O	
		144.7–350.0	343.4	12.6 (13.25)	Loss of H_2O+2(CH_3O)	
		326.7–442.0	375.1	20 (19.38)	Loss of C_8H_7N	
		451.0–947.0	578.0	22.6(22.7)	Loss of $C_5H_{15}NO_3$	41.8(41.69) MnO + 15C
$VO^{IV}(L)_2 \bullet 2H_2O$	4	50.5–91.8	70.7	5.5(5.84)	Loss of $2H_2O$	
		190.0–250.0	222.3	12.7(12.34)	Loss of C_6H_4	
		269.5–438.9	382.6	21.6(21.93)	Loss of C_8H_9NO	
		452.4–528.9	491.0	18.7(19.01)	Loss of $C_2H_{15}NO4$	41.5(40.79) VO_2 + 14C

300.0 °C, clearly indicates a weight loss centered at the peak temperature of 242.0 °C with 17.7%. This decomposition process is attributed to the removal of the methoxyphenyl moiety, theoretically calculated as 18.15%. As for the weight loss evaluated to13.00% seems to corroborate with the third decomposition representing the loss of phenyl moiety, theoretically calculated as 12.89%. Regarding the last process evidenced at 557.4 °C on the DTG curve (24.20% loss), it seems to be due to the removal of the organic entity ($C_3H_{17}N_2O_4$), theoretically calculated as 24.60%. Finally, the remaining final residue is identified as NiO-oxide with 16 carbon atoms [38].

For the manganese complex (Fig. 4B), the first decomposition ranges between 138.6–222.5 °C and it involves a weight loss of 3.00%, indicating the removal of one molecule of water, theoretically calculated to 2.98%. The second decomposition step, observed between 144.7 and 350.0 °C, shows a weight loss of 12.60%. This, being explained by the removal of second molecule of water accompanied with two methoxy (–OCH_3) moieties of the ligand corresponding to the weight loss of 13.25%, theoretically calculated. The next step decomposition, observed in the temperatures ranging from 326.0 to 442.0 °C implies a weight loss of 20.00%, probably due to the decomposition of the C_8H_7N corresponding to 19.38%, theoretically calculated. As for the last step, occurring in the temperatures range of 451.0–947.0 °C, caused 22.60% of weight loss. This loss may be imputed from the account of the remaining organic part ($C_5H_{15}NO_3$). So, these four degradation stages were denoted by the DTG peaks at 181.6, 343.4, 375.1 and 578.9 °C, respectively. The final residue may be manganese oxide (MnO), with carbon atoms (15C) [39].

Finally, the thermal decomposition of the vanadium complex (Fig. 4C) displays also four decomposition steps like its previous analog of manganese complex. These four steps occur in the following temperature ranges of 50.5–91.8, 190.0–250.0, 269.5–438.9 and 452.4–528.9 °C. Their DTG peaks were successively observed at 70.7, 222.3, 382.6 and 491.0 °C, respectively. A weight loss of 5.50% was noted for the first decomposition step corresponding to the release of two water molecules, as previously mentioned for the manganese complex. The second one induced a weight loss of 12.70% indicating as well the loss of the phenyl group, theoretically estimated to 12.34%. Considering these processes, previously observed for the nickel and manganese complexes, the obtained results allowed to suggest the presence of obvious similarities in the thermal decomposition pathway of all the complexes. However, the last decomposition step of the vanadium complex allowed to evaluate the loss weight to 41.50% as residue as VO_2 with 14 carbon atoms [40].

3.4. Electrochemical behavior

Cyclic voltammetry measurements were carried out to investigate the redox properties of the synthesized complexes. Fig. 5 displays the voltammetric curves of the nickel complex in the potential range varies from +1.6 to −2.2 V whereas for the manganese complex was between +1.4 and −1.4 V.

In the case of the nickel complex (see Fig. 5A), the voltammogram displays four redox processes. When the electrode potential is scanned towards negative values, a reduction peak is observed at −1.53 V, and its corresponding oxidation pair appears in the reverse scan at −1.38 V (ΔE= Epa - Epc = 150 mV). The anodic to cathodic peak current density ratio (Ipa/Ipc) of this process is closely equal to unity. This is assigned to the metal centered Ni^{II}/Ni^{I} redox couple [41,42]. Next, the reduction at −1.91 V, with a small oxidation counterpart −1.71 V can be attributed to the irreversible reduction of azomethine group. When the electrode potential is scanned from 0.0 to +1.60 V, the complex exhibits a large oxidation current from ca. +0.5 V. A reduction couple is discerned in the reverse scan, so the process is characterized by an $E_{1/2}$ = +0.65 V and peak separation about ΔE =180 mV, and can be assigned to the Ni^{III}/Ni^{II} redox couple [43]. Finally, an oxidation process is clearly observed at +1.34 V, which could probably be assigned to an oxidation of Schiff-base ligand [44].

The cyclic voltammogram of manganese complex (Fig. 5B) exhibits only one quasi-reversible redox couple with an anodic–cathodic peak separation (ΔE) equal to 200 mV. Its half wave potential value was then calculated as average of the anodic and cathodic peak potentials, which is found to be equal to $E_{1/2}$ = −0.49 V. These results suggest that this redox process may be described to Mn^{III}/Mn^{II} [45]. On the other hand, the wave at Epa = +1.12 V may probably correspond to the Schiff base ligand oxidation [44].

Cyclic voltammetry of the $V^{IV}O(L)_2 \bullet 2H_2O$ complex (see Fig. 5C) was performed in the potentials range varying from −1.0 to 1.5 V vs. SCE. This voltammogram displays two redox processes. The reduction peak for the first redox couple is observed at −0.74 V as half-wave potentials, whereas its corresponding oxidation pair appears in the reverse scan at −0.53 V, being the peak-to-peak separation equal to ΔE = 210 mV. According to literature, this redox process may be ascribed to V^{III}/V^{IV} [46]. For the second couple (See a magnified voltammogram in the inset of Fig. 5C), the cathodic peak is centered at Epc= +0.2 V vs. SCE, while the anodic one, it

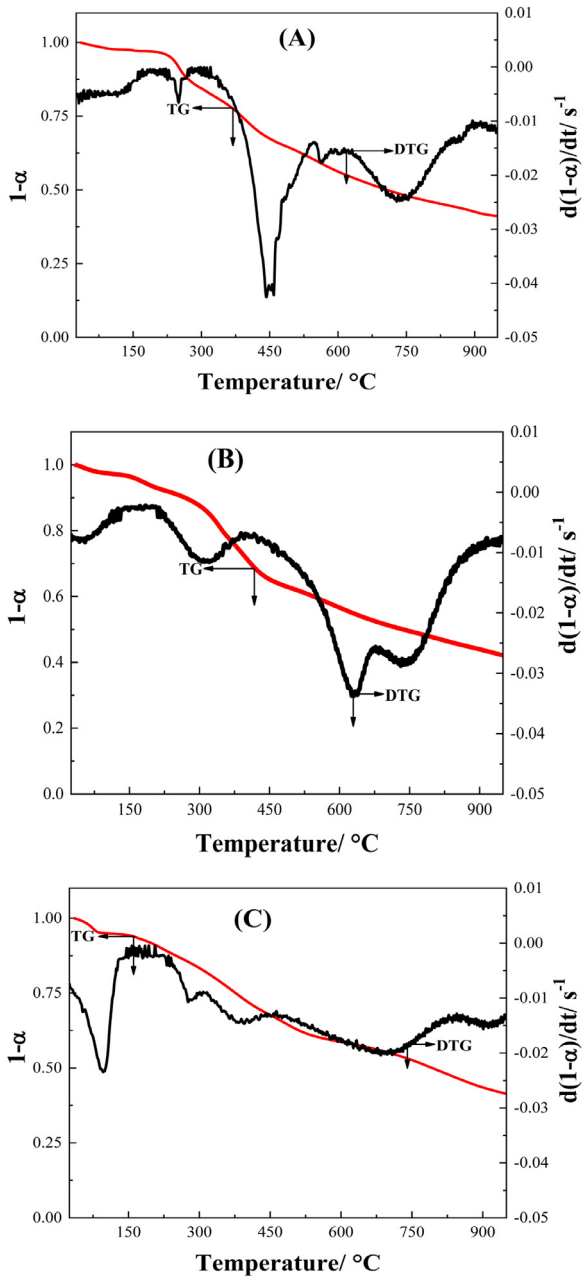

Fig. 4. The TG and DTG of **(A)**- Ni(II), **(B)-** Mn(II) and **(C)-** VO(IV) Schiff base complexes (where α, is the conversion = 1-w/w_0, w = the residual weight in mg and w_0 is the initial weight of the sample in mg).

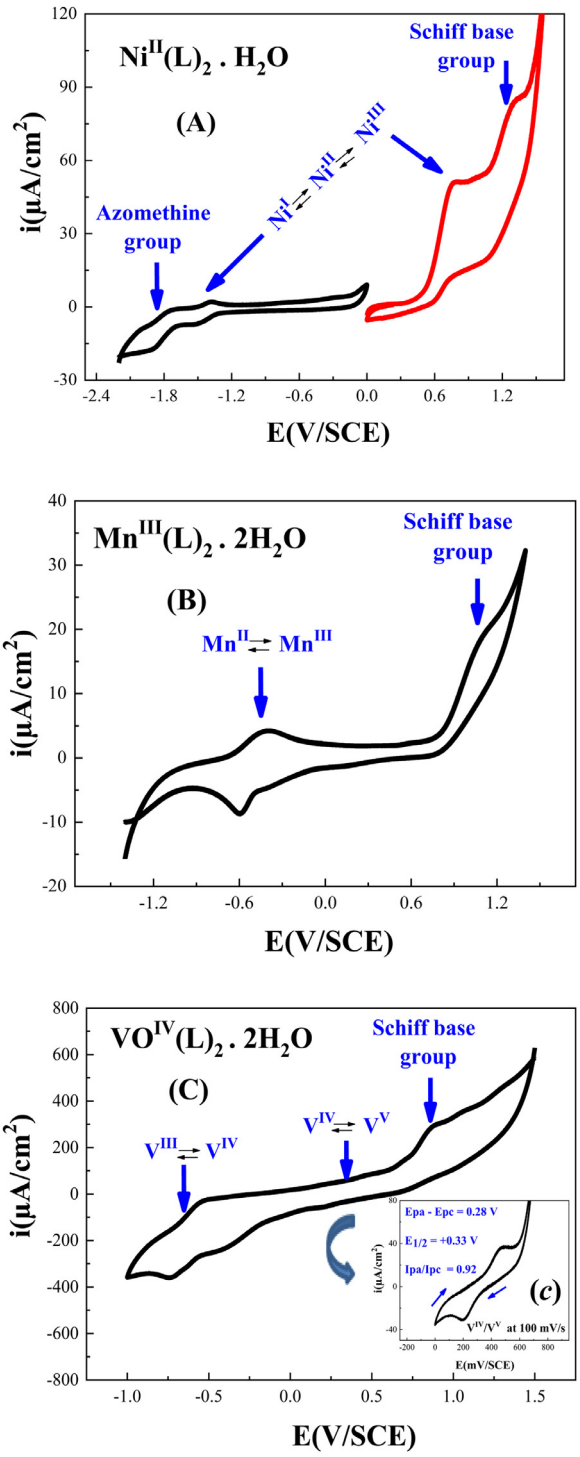

Fig. 5. Cyclic voltammograms of a GC electrode in an electrolytic solution containing 10^{-3} M Ni(II) (**A**), idem for Mn(II) (**B**) and VO(IV) (**C**) Schiff base complexes and 0.1 M of $TBABF_4$ in DMSO, under argon atmosphere and 100 mV/s as scan rate.

was seen at Epa = +0.48 V vs. SCE. This process has also been attributed to the V^{IV}/V^{V} redox couple [47] and it is characterized by ΔE = 0.28 V as peak to peak separation with a ratio Ipa/Ipc almost equal to unity (0.92) and $E_{1/2}$ = +0.33 V. These two redox systems of the vanadium complex are proposed to be monoelectronic transfer. The last oxidation wave observed at Epa = +0.82 V may probably due to the Schiff base ligand oxidation [44].

3.4.1. Effect of scan rate on the response of the Ni(II) complex

The cyclic voltammogram of the nickel complex in DMSO electrolytic solution under the potentials range going from −0.8 to −1.7 V shows a well-defined redox system (Fig. 6A) of the Ni(II)/Ni(I) species. Specifically, the Epa is equal −1.33 V and the cathodic peak is centered at −1.47 V. So, this redox couple shows a peak-to-peak separation (ΔE) is equal to 130 mV, and the ratio of Ipc/Ipa is practically equal to unity (1.01), suggesting an electrochemical process involving only one electron.

The reversibility of the Ni(II)/Ni(I) redox couple for the synthesized nickel complex was investigated using cyclic voltammetry at different scan rates. Fig. 6B depicts the voltammograms of the complex varying the scan rate between 25 and 500 mV s^{-1}. As it can be observed in this figure, the reversibility of the redox couple is well maintained even up to 500 mV s^{-1}. The effect of the scan rate on the electrochemical parameters associated to

Table 4
Electrochemical parameters obtained from cyclic voltammograms of Fig. 6.

$\lvert I_{Pa}/I_{Pc}\rvert$	0.95	0.97	1.02	1.01	1.02	1.03	1.01	1.01
ΔE (mV)	100	130	137	140	160	180	210	220
$E_{1/2}$ (mV)	−1400	−1405	−1407	−1410	−1415	−1418	−1422	−1425

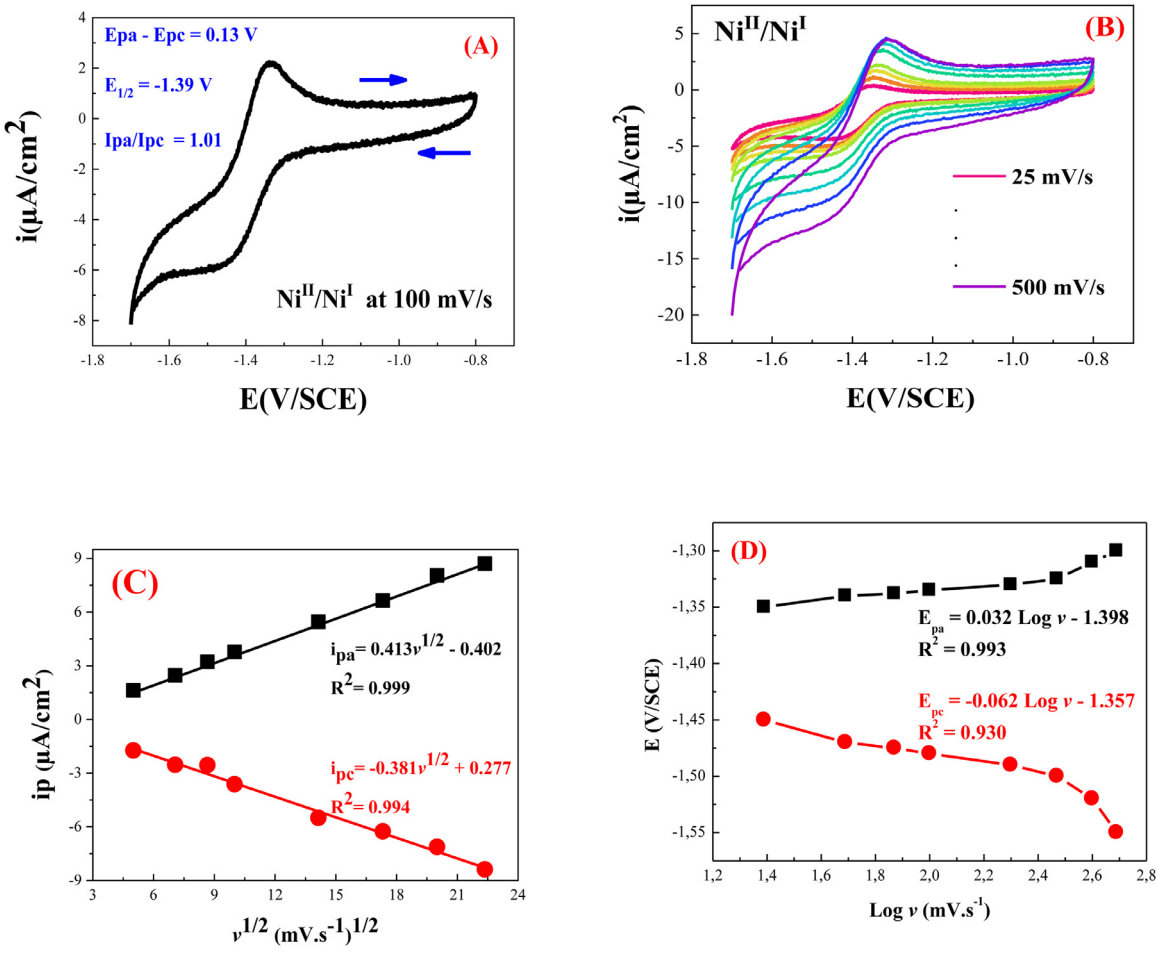

Fig. 6. (**A**) Cyclic voltammogram of the synthesized Ni(II) complex (10^{-3} M) in 0.1 M $TBABF_4$/DMSO at a scan rate of 100 mV s^{-1}; (**B**) Cyclic voltammograms of the same complex at different scan rates; **(C)** Plot of the cathodic and anodic peak currents versus the square root of sweep rate ($v^{1/2}$) and **(D)** Anodic and cathodic potentials versus Log v.

this redox couple are summarized in the Table 4, whereas Fig. 6C and D plot the cathodic and anodic peak current densities versus the square root of the scan rate ($v^{1/2}$) and the corresponding peak potentials versus the logarithm of the scan rate (Log v), respectively. The obtained results revealed a linear relationship between the peak current densities and $v^{1/2}$ (Fig. 6C). In addition, the anodic and cathodic peak potentials are found to be proportional to the Log v (Fig. 6D). These behaviors are indicative of a diffusion-controlled electron transfer process [48].

3.5. DFT calculations for the ligand and structures of the complexes

3.5.1. Geometry optimization

Geometry Optimization was done using B3LYP functional with 6–31G(d,p) basis sets as incorporated in the Gaussian 09 W program in gas phase. The fully optimized geometries of the ligand HL and its corresponding complexes are shown in Fig. 7. The numbering scheme for ligand HL, and complexes Ni(II), VO(IV) and Mn(II) are given in Scheme 3. Some selected optimized and values of bond lengths and angles obtained from DFT calculations are listed in Table 5.

HL ligand was optimized to investigate the geometric and electronic characteristics that may control its electrons donation. The optimized structure of ligand HL is distorted planar and two donating groups (hydroxyl and imino functional groups) which are facing each one to other around the central point of the molecule (Fig 7a). The C–O bond lengths in the complexes are significantly longer than that in the ligand as the result of the deprotonation of the phenolic groups. On the other hand, the N=C (azomethine) bond lengths are slightly shorter than that in the ligand. Other bond lengths and angles are rather in normal ranges and comparable with those reported by Ruchi Srivastava et al. [49]. The nickel complex is formed via nitrogen and phenolic oxygen atoms to form a square planar geometry. Both phenolic OH groups were deprotonated. The nitrogen atoms are in trans position towards oxygen atoms. The trans N–Ni-O angles are about 95° and the *cis* angles about the central Ni atom between 87.21 and 103.27 ° indicating a distorted square planar geometry. When optimizing Ni^{2+} ion com-

Table 5
Some important bond lengths (A°) and angles (°) of **HL** and its complexes.

Bond length (A°) /angle (°) HL		Bond length (A°) /angle (°) Ni(II)		Bond length (A°) /angle (°) VO(IV)		Bond length (A°) /angle (°) Mn(II)	
O29-C24	1.2897	O16-C10	1.3113	O15-C9	1.5131	O27-C9	1.5598
O34 –C19	1.3904	O48-C42	1.3113	O48-C41	1.4635	O25-C16	1.5634
N17-C16	1.4675	N2-C4	1.3165	N1-C3	1.3275	N5-C4	1.1346
N17-C18	1.3272	N2-C21	1.3148	N1-C28	1.4741	N5-C29	1.4743
O29-H31	1.7523	O15-H17	0.9924	O40-H16	0.956	O60-H62	0.9605
C18-C23	1.4075	C21-C27	1.5133	C19-C31	1.5702	C9-C27	1.5598
-	-	Ni1-N2	1.8117	VO67-N1	1.8722	Mn1-N2	1.8324
-	-	Ni1-O16	1.8006	VO67-O15	1.8527	Mn1-O25	1.5083
-	-	Ni1-O49	1.8007	VO67-O48	1.9283	Mn1-O27	1.992
C1-C16-C17	112.53	N2-C21-Ni1	119.4527	N1-C3-VO67	116.36	N5-C4- Mn1	84.71
C24-O29-H31	104.38	N2-Ni1-N3	103.2792	N1-VO67-N2	81.697	N5-Mn1-N2	92.64
C23-C24-O28	121.81	O16-Ni1-O49	87.2108	O15-VO67-O48	89.53	O26-Mn1-O27	91.28
C23-C18-N17	123.53	Ni1-N2-O16	95.2475	VO67- N1-O15	108.26	Mn1-N2-O27	91.06
C18-H28-C23	119.02	Ni1-N3-O49	95.2472	N2-VO67-O48	94.74	Mn1-N5-O26	93.52

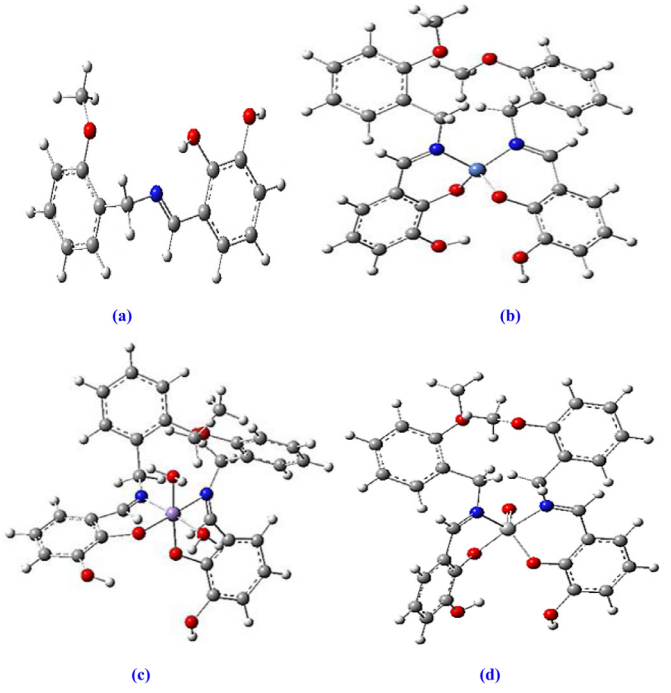

Fig. 7. Geometry Optimized structures of **(a)** Ligand HL, **(b)** Complex Ni(II), **(c)** Complex Mn(II), **(d)** Complex VO(IV) (Colour Code: H=White, C=gray, N=Blue, O= red, Ni=Silver gray, VO= gray, Mn=Purple).

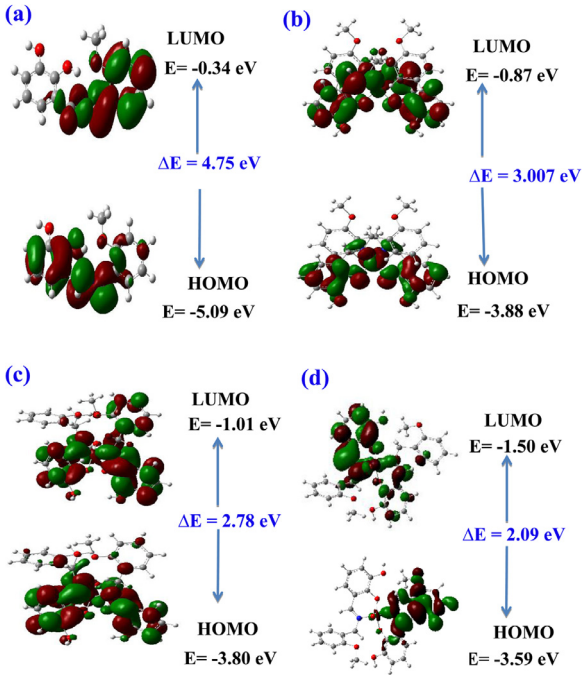

Fig. 8. Presentation of the energy levels, energy gaps, and frontier molecular orbitals of **(a)** Ligand HL, **(b)** Complex Ni(II), **(c)** Complex Mn(II), **(d)** Complex VO(IV).

plex with HL Schiff base ligand, the lowest energy structure has a square planar geometry with molecular formula $[Ni^{II}(L)_2 \bullet H_2O]$. This geometry is accomplished with the protonation of the hydroxyl groups to neutralize the Ni^{2+} ion. The stability of this complex came from the formation of two four membered rings between Ni and ligand (Fig. 7b). While the ligand formed 1:1 complex with acetate salts of manganese and vanadium through coordination via nitrogen and phenolic oxygen atoms to form octahedral geometry and square-pyramidal around the central metal ions Mn(II) and VO(IV) complexes, respectively. the optimized structure of $Mn^{2+}$was octahedral, however the ligand was deprotonated within the coordination and the octahedral geometry was fulfill by two water molecules. Optimization results showed that water molecules coordinated in a plane perpendicular to the Mn-HL plane Fig. 7c. In addition, it has been observed that in Mn(II) complex also the donor groups of the ligand were coordinated with the metal center in one plane. Although, VO^{2+} ion formed square-pyramidal $[V^{IV}O(L)_2 \bullet 2H_2O]$ complex with HL Schiff base ligand, where the ligand donor groups coordinated in one plane with VO. To prevent the steric effect that occurred between VO^{2+} and hydroxyl groups of HL, since the protons rotate in the opposite directions as shown in Fig. 7d.

3.5.2. Orbital frontiers (FMOS)

The frontier orbitals HOMO and LUMO are the main orbitals that can provide information on the chemical stability helping to better understanding the properties governing the electronic excitation. HOMO is the orbital that acts as an electron donor whereas LUMO is an orbital acting as electron acceptor. The energy values of HOMO and LUMO with their energy gap reflect the chemical reactivity of a molecule [50]. So, Fig. 8 shows the distributions and energy levels of the HOMO and LUMO orbitals, computed with the B3LYP/6–31G(d,p) level for the ligand HL and its complexes. As shown in Fig. 8, the positive region is presented in red and the negative one in green. The Table 6 summarizes the HOMO and LUMO energies and some related physicochemical parameters characteristic (energy gap, ΔE, electronic chemical potential (μ), hardness (η) and electrophilicity (ω)) of Schiff base ligand

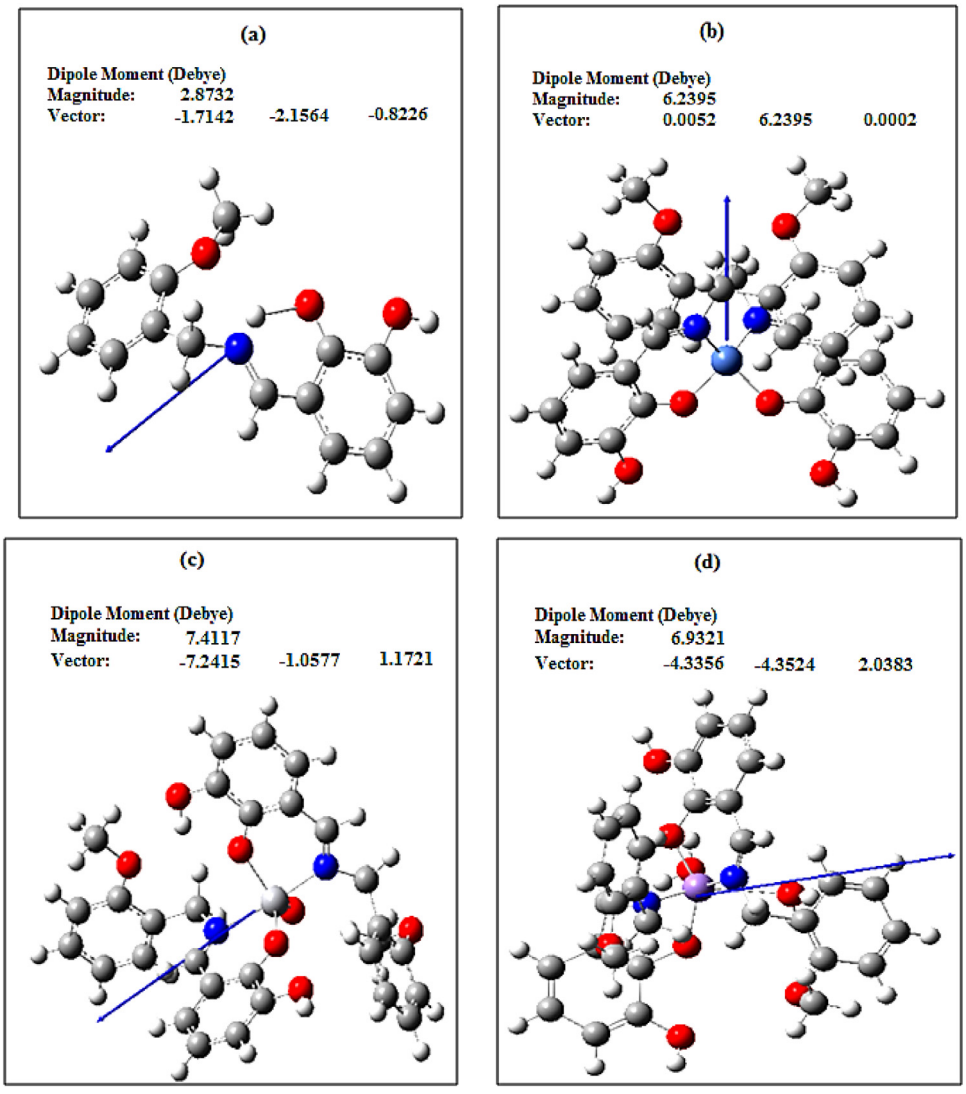

Fig. 9. Direction of dipole moment of Ground state optimized structures of **(a)** Ligand HL, **(b)** Complex Ni(II), **(c)** Complex VO(IV), **(d)** Complex Mn(II).

Table 6
Calculated HOMO, LUMO, energy gap (ΔE), chemical hardness (η), electronic chemical potential (μ) and electrophilicity (ω) of the ligand and its corresponding Ni(II), VO(IV) and Mn(II) complexes. All values were calculated in eV unit.

Compound	HOMO	LUMO	ΔE	η	μ	ω
HL	−5.09	−0.34	4.75	2.37	−2.71	1.54
Ni(II)	−3.88	−0.87	3.06	1.53	−2.37	1.83
VO(IV)	−3.59	−1.50	2.09	1.04	−2.54	2.53
Mn(II)	−3.80	−1.01	2.78	1.39	−2.40	2.11

$\eta = 1/2(E_{LUMO}\text{-}E_{HOMO})$, $\mu = 1/2(E_{HOMO} + E_{LUMO})$, $\omega = \mu^2/2\eta$.

HL with its complexes. Chemical hardness is associated to the stability and reactivity of a chemical system. According to the frontier molecular orbitals, chemical hardness corresponds to the energy gap between HOMO and LUMO. As the energy gap increases, the molecule becomes harder and more stable/less reactive. Thus, there is short gap between HOMO and LUMO in the complexes as compared to their ligand. The values of electronic chemical potential of Schiff base ligand HL and its complexes are presented in Table 6, the greater electronic chemical potential (absolute values), the less stable or more reactive. The electrophilicity ($\boldsymbol{\omega}$) index has become a powerful tool for the study of the reactivity of organic molecules participating in polar reactions [51]. The electrophilicity index measures the easiness of a species to accept electrons. A good electrophile is characterized by a high value of ($\boldsymbol{\omega}$) but, in the opposite case, a good and more reactive nucleophile is rather characterized by a low value of ($\boldsymbol{\omega}$). So, the electrophilicity ($\boldsymbol{\omega}$) scale allowed the classification of organic molecules as strong electrophiles with $\boldsymbol{\omega} > 1.5$ eV, moderate electrophiles with $0.8 < \boldsymbol{\omega} < 1.5$ eV and marginal electrophiles with $\boldsymbol{\omega} < 0.8$ eV [52]. Table 6 indicates that the all complexes are stronger electrophiles with $\boldsymbol{\omega} > 1.5$ eV. The value of ($\boldsymbol{\omega}$) for HL, Ni(II), Mn(II) and VO(IV) are 1.54, 1.83, 2.11 and 2.53 eV, respectively. Therefore, it can be concluded that these complexes are the stronger electrophiles and electron acceptors than their HL ligand which is easily acting as a good electron donor and more reactive nucleophile.

3.5.3. Electric moments

The dipole moment in a molecule is of an important property, which is defined as the first derivative of the energy with respect to an applied electric field. It is mainly used to explore the intermolecular interactions such as van der Waals type dipole-dipole forces etc. The larger dipole moment will be the stronger intermolecular attraction [53]. Total dipole moment is very important indicator in the reaction mechanisms since it expresses the ability

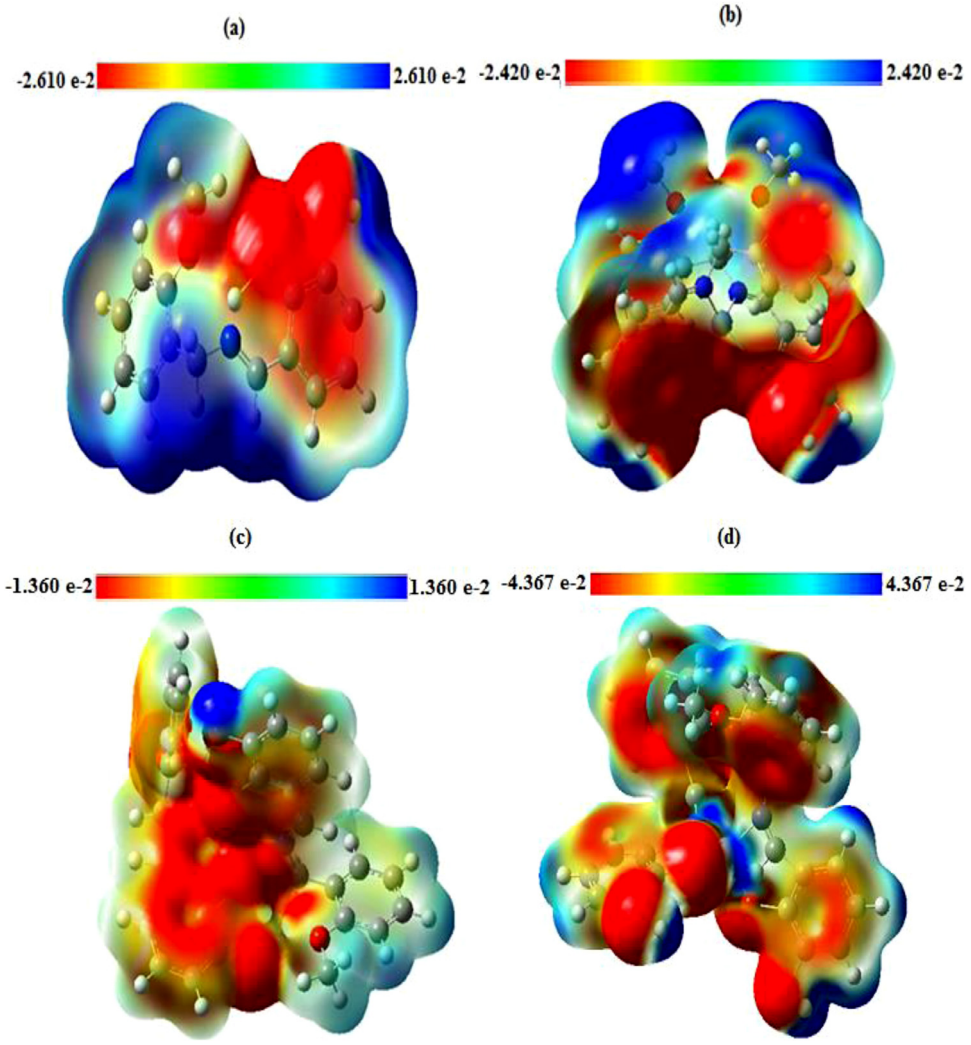

Fig. 10. Molecular electrostatic potential maps of **(a)** Ligand HL, **(b)** Complex Ni(II), **(c)** Complex VO(IV), **(d)** Complex Mn(II) at the B3LYP/6–31G(d,p) level of theory.

of the molecule to interact with the other molecules founding in its surrounding space.

The calculated parameters above described and the electronic dipole moment {**μi** ($i = x$, y, z) with the total dipole moment **μtot**} for Schiff base ligand HL and Ni(II), Mn(II) and VO(IV) complexes are listed in Table 7. Our calculated results have showed that the ligand and its complexes possess a dipole moment of 2.8732 (HL), 6.2395 (Ni(II)), 6.9321 (Mn(II)) and 7.7547 (VO(IV)) D(Debye) for B3LYP which indicates a high reactivity to interact with the surrounding media. The calculated results showed that VO(IV) has the highest value of dipole moment than all the other compounds (Fig. 9).

3.5.4. Nonlinear optical (NLO) properties

Nonlinear optical (NLO) effects arise from the interactions of electromagnetic fields in various media to produce new fields altered in phase, frequency, amplitude or other propagation characteristics from the incident fields [54]. Some quantum chemical descriptors which are the mean polarizability (α), the anisotropy of the polarizability ($\Delta\alpha$) and first order hyperpolarizability (β) have been used for explaining the NLO properties in many computational studies [55]. In the present study, the molecular polarizability, anisotropy of polarizability and molecular first hyperpolarizability of HL and its complexes were investigated by using B3LYP/6–31G(d,p) approaches within the density functional theory

Table 7
The B3LYP/6–31G(d,p) calculated electric dipole moments (Debye), polarisability (in a.u), ß components and ß tot value of HL, Ni(II), VO(IV) and Mn(II) complexes.

Parameters	HL	Ni(II)	VO(IV)	Mn(II)
μ_x	−2.4198	2.1894	−5.0781	−5.6321
μ_y	−2.6969	2.0836	−5.8607	−3.1826
μ_z	0.4168	2.0253	−0.0150	2.4910
$\boldsymbol{\mu_{tot}}$	**2.8732**	**6.2395**	**7.7547**	**6.9321**
α_{xx}	−99.9058	−205.1184	−247.6975	−214.1616
α_{yy}	−96.0414	−210.9704	−232.5401	−220.8387
α_{zz}	−109.8336	−225.7951	−231.2249	−226.6761
α_{xy}	2.7832	0.8714	11.4563	9.8801
α_{xz}	1.4939	8.0543	−16.0336	17.3521
A_{yz}	−0.2142	−10.1195	17.7394	15.3022
$< \alpha >$	**−101.9278**	**−213.9613**	**−237.1541**	**−220.558**
$\Delta\ \alpha°$	**13.5248**	**29.1536**	**48.7295**	**45.0485**
$ß_{xxx}$	64.8155	64.8155	−274.9187	−0.8224
$ß_{xxy}$	−13.9245	−13.9245	−132.9412	−24.9312
$ß_{xyy}$	−8.9802	−8.9882	16.3759	−43.6176
$ß_{yyy}$	15.4898	15.4898	100.6738	166.7716
$ß_{xxz}$	−39.0351	−39.0351	31.0844	−10.8502
$ß_{xyz}$	−6.7001	−6.7001	67.2330	−18.6250
$ß_{yyz}$	4.7512	4.7512	3.6709	−4.9014
$ß_{xzz}$	−13.9245	−13.9245	27.0438	−6.0415
$ß_{yzz}$	8.4708	8.4708	−11.9078	−48.6632
$ß_{zzz}$	6.8008	6.8008	34.4736	−44.3838
$\boldsymbol{ß_{tot}}$	**51.1132**	**51.1066**	**245.1870**	**123.8642**

are listed in Table 7. Polarizability characterizes the ability of an electric field to distort the electronic distribution of a molecule. Higher order polarizabilities (hyperpolarizabilities) which describe the nonlinear response of atoms and molecules are related to a wide range of phenomenon from nonlinear optics to intermolecular forces, such as the stability of chemical bonds as well as the conformation of molecules and molecular aggregates [56].

The calculated of the polarizability, the anisotropy of the polarizability and first order hyperpolarizability for Schiff base ligand HL and Ni(II), Mn(II) and VO(IV) complexes are listed in Table 7. To present calculations, the mean polarisability and anisotropy of polarizability of VO(IV) is found higher than the other compounds, calculated at the same level of theory as well as same basis set 6–31G(d,p). This is related very well to the smaller frontier orbital energy gap of oxovanadium (IV) as compared to other compounds. The total first hyperpolarisability value <ßtot> of the title compounds is equal to 51.1132, 51.1066, 123.8642 and 245.1870 (a.u) for HL and Ni(II), Mn(II) and VO(IV), respectively. The results indicate that the complex of VO(IV) possesses better nonlinear optical properties and is a potential candidate for nonlinear optical applications than the other compounds.

3.5.5. Molecular electrostatic potential (MEP)

The MEP is a useful property to study the attacking sites for electrophilic and nucleophilic substitution reactions [57,58]. The total electron density surface mapped with electrostatic potential for the ligand HL and their complexes as shown in Fig. 10. The different values of the electrostatic potential at the surface are represented by different colors. The corresponding mapped electrostatic potential is indicated by red color, the negative regions represented by the red color are the preferable sites for electrophilic attack. Here, the negative potentials are generated over the electronegative oxygen and nitrogen atoms whereas the H-atoms have a positive potential region in the structures and the positive regions represented by the blue color are favorable sites for nucleophilic attack. This last is centered around hydrogen and carbon atoms. The yellow regions indicate the slightly rich electron and the green regions indicate neutral.

4. Conclusion

In summary, we have successfully synthesized and characterized three new Schiff-base complexes of nickel(II), manganese(II) and oxovanadium(IV). From the results of FT-IR, UV-Vis, LC-MS and elemental analysis, the molecular structures of the complexes have been proposed. The bis-bidentate Schiff-base ligands coordinate to the VO(IV), Mn(II) and Ni(II) ions in a tetradentate mode (ML_2) using the azomethine N and enol O atoms. The assignment of a square-planar geometry for Ni(II), a square-pyramidal geometry for the VO(IV) and an octahedral geometry for the Mn(II), is supported by electronic absorption and infrared spectral measurements, as well as quantum chemical calculations. The electrochemical characterization shows that the complexes exhibit redox activity associated to their metal centers. Moreover, the calculated molecular properties suggest that the VO(II) complex may be the most stable compound and that exhibiting best NLO properties. Hence, the present study shows a simple method for the synthesis of some bis-bidentates Schiff base complexes with interesting properties to be used in electrochemical and other applications.

Declaration of Competing Interest

The authors declare that they have no known competing financial interests or personal relationships that could have appeared to influence the work reported in this paper.

CRediT authorship contribution statement

Djouhra Aggoun: Writing - original draft, Investigation, Conceptualization, Methodology, Validation, Formal analysis, Data curation, Supervision. **Zakia Messasma:** Data curation, Writing - review & editing, Validation. **Brahim Bouzerafa:** Writing - review & editing, Validation, Investigation. **Raúl Berenguer:** Writing - review & editing, Resources, Validation. **Emilia Morallon:** Writing - review & editing, Validation. **Yasmina Ouennoughi:** Writing - review & editing, Validation. **Ali Ourari:** Validation, Writing - review & editing, Supervision.

Acknowledgments

The authors would like to thank the MESRS and DG-RSDT (Ministère de l'Enseignement Supérieur et de la Recherche Scientifique et la Direction Générale de la Recherche et du Développement Technologique-Algérie) for their financial support. Financial support from the Ministerio de Economía y Competitividad (Spain) and FEDER (MAT2016-76595-R and RYC-2017-23618) is also gratefully acknowledged.

References

[1] H. Schiff, Untersuchungenüber Salicinderivate, Ann. Chem. 150 (1869) 193–200.
[2] V.M. Leovac, D.M. Joksovic, V. Divjakovic, L.S. Jovanovic, Z. Saranovic, A. Pevec, Synthesis, spectroscopic and X-ray characterization of a copper(II) complex with the Schiff base derived from pyridoxal and aminoguanidine: NMR spectral studies of the ligand, J. Inorg. Biochem. 101 (2007) 1094–1097.
[3] a) E.N. Jacobsen, M.H. Wu, in: H. Yamamoto (Ed.), Comprehensive Asymmetric Catalysis: Asymmetric Synthesis and Induction Catalysts, 2, Springer, Berlin, 1999, pp. 649–677; b) T. Katsuki, in: I. Ojima (Ed.), Wiley-VCH, New York, 2000, pp. 287–325; c) E.N. Jacobsen, in: I. Ojima (Ed.), VCH, New York, 1993, pp. 159–202.
[4] a) J. Tisato, F. Refosco, F. Bandoli, Structural survey of technetium complexes, Coord. Chem. Rev. 135 (1994) 325–397; b) I.N. Booysen, S. Maikoo, M.P. Akerman, B. Xulu, Novel ruthenium (II) and (III) compounds with multidentate Schiff base chelates bearing biologically significant moieties, Polyhedron 79 (2014) 250–257.
[5] D. Aggoun, A. Ourari, R. Ruiz-Rosas, E. Morallon, A selective naked-eye chemosensor derived from 2-methoxybenzylamine and 2,3-dihydroxybenzaldehyde: synthesis, spectral characterization and electrochemistry of its bis-bidentates Schiff bases metal complexes, Spectrochim. Acta A 184 (2017) 299–307.
[6] A.A. Alshaheri, M.I.M. Tahir, M.B. Abdul Rahman, T. Begum, T.A. Saleh, Synthesis, characterization and catalytic activity of dithiocarbazate Schiff base complexes in oxidation of cyclohexane, J. Mol. Liq. 240 (2017) 486–496.
[7] A. Ourari, M. Khelafi, D. Aggoun, A. Jutand, C. Amatore, Electrocatalytic oxidation of organic substrates with molecular oxygen using tetradentate ruthenium(III)-Schiff base complexes as catalysts, Electrochim. Acta 75 (2012) 366–370.
[8] F. Heshmatpour, S. Rayati, M.A. Hajiabbas, P. Abdolalian, B. Neumüller, Copper(II) Schiff base complexes derived from 2,20-dimethyl-propandiamine: synthesis, characterization and catalytic performance in the oxidation of styrene and cyclooctene, Polyhedron 31 (2012) 443–450.
[9] A. Ghaffari, M. Behzad, M. Pooyan, H.A. Rudbari, G. Bruno, Crystal structures and catalytic performance of three new methoxy substituted salen type nickel(II) Schiff base complexes derived from meso-1,2-diphenyl-1,2-ethylenediamine, J. Mol. Struct. 1063 (2014) 1–7.
[10] S. Ilhan, H. Baykara, A. Oztomsuk, V. Okumus, A. Levent, M.S. Seyitoglu, S. Ozdemir, Synthesis and characterization of 1,2-bis(2-(5-bromo-2 hydroxybenzilidenamino)-4-chlorophenoxy) ethane and its metal complexes: an experimental, theoretical, electrochemical, antioxidant and antibacterial study, Spectrochim. Acta A 118 (2014) 632–642.
[11] S. Mohebbi, S. Eslami, Electrocatalytic oxidation of 2-mercaptoethanol using modified glassy carbon electrode by MWCNT in combination with unsymmetrical manganese (II) Schiff base complexes, Mate. Res. Bull. 66 (2015) 219–225.
[12] C.R. Bhattacharjee, P. Goswami, M. Sengupta, Synthesis, electrochemical and antimicrobial studies of mono and binuclear iron(III) and oxovanadium(IV) complexes of [ONO] donor tridentate Schiff-base ligands, J. Coord. Chem. 63 (2010) 3969–3980.
[13] A. Kamath, N.V. Kulnarni, P.P. Netalkar, V.K. Revankar, Phenoxide bridged tetranuclear Co(II), Ni(II), Cu(II) and Zn(II) complexes: electrochemical, magnetic and antimicrobial studies, Spectrochim. Acta A 79 (2011) 1418–1424.
[14] K.C. Gupta, A.K. Sutar, Catalytic activities of Schiff base transition metal complexes, Coord. Chem. Rev. 252 (2008) 1420–1450.
[15] D.A. Atwood, M.J. Harvey, Group 13 compounds incorporating Salenligands, Chem. Rev. 101 (2001) 37–52.

[16] N. Yoshida, K. Ichikawa, M. Shiro, Supramolecular motifs in metal complexes of Schiff bases. Part 5. Zinc(II)-assisted self-assembly of some bis-*N,N*- and *N,O*-bidentate Schiff bases and chiral packing modes in solid state, J. Chem. Soc., Perkin Trans. 2 (2000) 17–26.
[17] H. Hosseini-Monfared, R. Bikas, P. Mahboubi-Anarjan, A.J. Blake, V. Lippolis, N.B. Arslan, C. Kazak, Oxidovanadium(V) complexes containing hydrazone based O,N,O-donor ligands: synthesis, structure, catalytic properties and theoretical calculations, Polyhedron 69 (2014) 90–102.
[18] A. Ourari, I. Bougossa, S. Bouacida, D. Aggoun, R. Ruiz-Rosas, E. Morallon, H. Merazig, Synthesis, characterization and X-ray crystal structure of novel nickel Schiff base complexes and investigation of their catalytic activity in the electrocatalytic reduction of alkyl and aryl halides, J. Iran. Chem. Soc. 14 (2017) 703–715.
[19] W. Kohn, L.J. Sham, Self-consistent equations including exchange and correlation effects, Phys. Rev. 140 (1965) 1133–1138.
[20] A.D. Becke, Density-functional thermochemistry. III. The role of exact exchange, J. Chem. Phys. 98 (1993) 648–5652.
[21] C. Lee, W. Yang, R.G. Parr, Development of the Colle-Salvetti correlation-energy formula into a functional of the electron density, Phys. Rev. 37 (1998) 785–789.
[22] B. Miehlich, A. Savin, A. Stoll, H. Preuss, Results obtained with the correlation energy density functionals of becke and Lee, Yang and Parr, Chem. Phys. Lett. 157 (1989) 200–206.
[23] B. Bouzerafa, A. Ourari, D. Aggoun, R. Ruiz-Rosas, Y. Ouennoughi, E. Morallon, Novel nickel(II) and manganese(III) complexes with bidentate Schiff-base ligand: synthesis, spectral, thermogravimetry, electrochemical and electrocatalytical properties, Res. Chem. Intermed. 42 (2016) 4839–4858.
[24] A. Ourari, D. Aggoun, Synthesis and spectral analysis of N-substituted pyrrole salicylaldehyde derivatives-electropolymerization of a new nickel(II)-Schiff base complex derived from 6-[3′-N-pyrrolpropoxy]-2 -hydroxyacetophenone and 1,2-diaminoethane, J. Iran. Chem. Soc. 12 (2015) 1893–1904.
[25] R. Aurkie, M.G. Rosair, R. Kadam, S. Mitra, Three new mono- di-trinuclear cobalt complexes of selectively and non-selectively condensed Schiff bases with N_2O and N_2O_2 donor sets: syntheses, structural variations. EPR DNA Bind Stud, Polyhedron 28 (2009) 796–806.
[26] R.N. Egekenze, Y. Gultneh, R. Butcher, Mn(III) and Mn(II) complexes of tridentate Schiff base ligands; synthesis, characterization, structure, electrochemistry and catalytic activity, Inorg. Chim. Acta 478 (2018) 232–242.
[27] A.M. Fayed, S.A. Elsayed, A.M. El-Hendawy, M.R. Mostafa, Complexes of cis–dioxomolybdenum(VI) and oxovanadium(IV) with a tridentate ONS donor ligand: synthesis, spectroscopic properties, X-ray crystal structure and catalytic activity, Spectrochim. Acta A 129 (2014) 293–302.
[28] B. Bouzerafa, D. Aggoun, Y. Ouennoughi, A. Ourari, R. Ruiz-Rosas, E. Morallon, M.S. Mubarak, Synthesis, spectral characterization and study of thermal behavior kinetics by thermogravimetric analysis of metal complexes derived from salicylaldehyde and alkylamine, J. Mol. Struct. 1142 (2017) 48–57.
[29] M. Salehi, F. Faghani, M. Kubicki, M. Bayat, New complexes of Ni(II) and Cu(II) with tridentate ONO Schiff base ligand: synthesis, crystal structures, electrochemical and theoretical investigation, J. Iran. Chem. Soc. 15 (2018) 2229–2240.
[30] M.M. Tulu, A.M. Yimer, Catalytic Studies on Schiff Base Complexes of Co(II) and Ni(II) Using Benzoylation of Phenol, Mod. Chem. Appl. 6 (2018) 1–6.
[31] M.R. Bermejo, M.I. Fernández, E. Gómez-Fórneas, A. González-Noya, M. Maneiro, R. Pedrido, M.J. Rodríguez, Self-assembly of dimeric MnII-I–Schiff-base complexes tuned by perchlorate anions, Eur. J. Inorg. Chem. (2007) 3789–3797.
[32] G. Gonzalez-Riopedre, M.I. Fernandez-Garcıa, A.M. Gonzalez-Noya, M.A. Vazquez-Fernandez, M.R. Bermejo, M. Maneiro, Manganese-Schiff base complexes as catalysts for water photolysis, Phys. Chem. Chem. Phys. 13 (2011) 18069–18077.
[33] M. Tűmer, Synthesis and spectral characterization of metal complexes containing tetra- and pentadentate schiff base ligands, Synth. React. Inorg. Met. Org. Chem. 30 (2000) 1139–1158.
[34] P.S. Prasad, P. Kumar, K. Bharathi, V. Narayanan, Synthesis of Vanadium (III) Schiff base complex and its electrocatalytic sensing application, Mechanics, Mater. Sci. Eng. (2017) 130–134.
[35] A.R. Cowley, J.R. Dilworth, P.S. Donnelly, A.D. Gee, J.M. Heslop, Acetylacetonate bis(thiosemicarbazone) complexes of copper and nickel: towards new copper radiopharmaceuticals, Dalton Trans. (2004) 2404–2412.
[36] B. Debajani, L.R. Ashray, K. Arvind, Synthesis, and characterization of low- and high-spin manganese(II) complexes of polyfunctional adipoyldihydrazone: effect of coordination of N-donor ligands on stereo-redox chemistry, J. Mol. Struct. 1092 (2015) 122–129.
[37] A.A. Hassoon, N.S. Al-Radadi, N. Nawar, M.M. Mostafa, New Square-Pyramidal Oxovanadium (IV) complexes derived from polydentate ligand (L1), J. Inorg. Chem. 6 (2016) 23–65.
[38] M. Ikram, S. Rehman, M. Ali, C.S. Faridoon, R.J. Baker, A.J. Blake, K. Malook, H. Wong, S. Ur-Rehman, Urease and α-chymotrypsin inhibitory activities of transition metal complexes of new Schiff base ligand: kinetic and thermodynamic studies of the synthesized complexes using TG–DTA pyrolysis, Thermochim. Acta 562 (2013) 22–28.
[39] E.M. Zayed, G.G. Mohamed, A.M.M. Hindy, Transition metal complexes of novel Schiff base Synthesis, spectroscopic characterization, and in vitro antimicrobial activity of complexes, J. Therm. Anal. Calorim. 120 (2014) 893–903.
[40] A.H. Kianfar, V. Sobhani, M. Dostani, M. Shamsipur, M. Roushani, Synthesis, spectroscopy, electrochemistry and thermal study of vanadyl unsymmetrical Schiff base complexes, Inorg. Chim. Acta 365 (2011) 108–112.
[41] M. Pooyan, A. Ghaffari, M. Behzad, H. Amiri Rudbari, G. Bruno, Tetradentate N_2O_2 type Nickel(II) Schiff base complexes derived from *meso*-1,2-diphenyle-1,2-ethylenediamine: synthesis, characterization, crystal structures, electrochemistry, and catalytic studies, J. Coord. Chem. 66 (2013) 4255–4267.
[42] D. Chatterjee, A. Mitra, Olefin epoxidation catalysed by Schiff-base complexes of Mn and Ni in heterogenised-homogeneous systems, J. Mol. Catal. A: Chem. 144 (1999) 363–367.
[43] N. Bréfuel, C. Lepetit, S. Shova, F. Dahan, J.-P. Tuchagues, Complexation to Fe(II), Ni(II), and Zn(II) of multidentate ligands resulting from condensation of 2-pyridinecarboxaldehyde with alpha, omega-triamines: selective imidazolidine/hexahydropyrimidine ring opening revisited, Inorg. Chem. 44 (2005) 8916–8928.
[44] J.L.N. Xavier, E. Ortega, J.Z. Ferreira1, A.M. Bernardes, V. Pérez-Herranz, An electrochemical Study of Phenol Oxidation in Acidic Medium, Int. J. Electrochem. Sci. 6 (2011) 622–636.
[45] M.H. Habibi, E. Askari, M. Amirnasr, A. Amiri, Y. Yamane, T. Suzuki, Syntheses, spectral, electrochemical and thermal studies of mononuclear manganese(III) complexes with ligands derived from 1,2-propanediamine and 2-hydroxy-3 or 5-methoxybenzaldehyde: self-assembled monolayer formation on nanostructure zinc oxide thin film, Spectrochim. Acta A 79 (2011) 666–671.
[46] K. Ramesh, T.K. Lal, R.N. Mukherjee, Synthesis, spectra and electrochemistry of Non-Oxovanadium(IV) bischelates of tridentate Schiff base ligands. Magnetism of Bis[N-(2-Hydroxyphenyl)-5- Methylsalicylideniminato]Vanadium(IV), Polyhedron 11 (1992) 3083–3089.
[47] P. Galloni, A. Coletti, B. Floris, V. Conte, Electrochemical properties of VO salen complexes, Inorg. Chim. Acta 240 (2014) 144–148.
[48] J.T. Lundquist, J.R., R.S. Nicholson, Theory of the potential step-linear scan electrolysis method with a comparison of rate constants determined electrochemically and by classical methods, J. Electroanal. Chem. 16 (1968) 445–456.
[49] R. Srivastava, L. Sinha, M. Karabacak, O. Prasad, S.K. Pathak, A.M. Asiri, M. Cinar, Spectral features, electric properties, NBO analysis and reactivity descriptors of 2-(2-Benzothiazolylthio)-Ethanol: combined experimental and DFT studies, Spectrochim. Acta A 136 (2014) 1205–1215.
[50] Y. Sun, X. Chen, L. Sun, X. Guo, W. Lu, Nanoring structure and optical properties of Ga8As8, J. Chem. Phys. Lett. 381 (2003) 397–403.
[51] P. Perez, L.R. Domingo, A. Aizman, R. Contreras, The electrophilicity index in organic chemistry, Theoretical Aspects of Chemical Reactivity, Ume 19, Elsevier, New York, NY, USA, 2007.
[52] L.R. Domingo, M.J. Aurell, P. Perez, R. Contreras, Quantitative characterization of the global electrophilicity power of common diene/dienophile pairs in Diels-Alder reactions, Tetrahedron 58 (2002) 4417–4423.
[53] M. Bouklah, H. Harek, R. Touzani, B. Hammouti, Y. Harek, DFT and quantum chemical investigation of molecular properties of substituted pyrrolidinones, Arab. J. Chem. 5 (2012) 163–166.
[54] M. Albota, D. Beljonne, J.L. Brédas, J.E. Ehrlich, J.Y. Fu, A.A. Heikal, S.E. Hess, T. Kogej, M.D. Levin, S.R. Marder, D. Mc Cordmaughon, J.W. Perry, H. Rockel, M. Rumi, C. Subramaniam, W.W. Webb, I.L. Wu, C. Xu, Design of organic molecules with large two-photon absorption cross sections, Science 281 (1998) 1653–1656.
[55] K.G. Krishnan, R. Sivakumar, V. Thanikachalam, H. Saleem, M. Arockia doss, Synthesis, spectroscopic investigation and computational study of 3-(1-(((methoxycarbonyl)oxy)imino)ethyl)-2H-chromen-2-one, Spectrochim. Acta Part A 144 (2015) 29–42.
[56] P.J. Stephens, K.J. Jalkanen, A new formalism for paramagnetic susceptibilities: CH_3F, J. Chem. Phys. 91 (1989) 1379–1382.
[57] J.S. Murray, K. Sen, Molecular Electrostatic Potentials, Concepts and Applications, Elsevier, Amsterdam, 1996.
[58] P. Politzer, D.G. Truhlar, Chemical Application of Atomic and Molecular Electrostatic Potentials, Plenum, New York, 1981.